scientific reports

Check for updates

OPEN

Asymmetric-bifurcation snapping, all-or-none motion of Venus flytrap

Xiangli Zeng, Yingzhe Wang & Keisuke Morishima✉

The Venus flytrap is a carnivorous plant that catches insects by snapping rapidly and reopening slowly. To understand the mechanism underlying this asymmetrically reversible motion, a three-dimensional laser profiler was used to measure both static morphological information and dynamic movements (500 frames per second) of the Venus flytrap, including its rapid closure and slow re-opening. The mean-curvature differences between the open and closed lobes were recorded and used for morphology and energy evaluations. The effects of geometric parameters such as the length, width, height, and thickness of the lobes on the closing time were analyzed, and the all-or-none motion of the Venus flytrap was examined. Moreover, a mathematical asymmetric-bifurcation buckling model was developed. The Venus flytrap has asymmetric energy states for the closing and opening conditions; therefore, storage of a larger amount of energy makes the re-opening motion slower. These pre-programmed movements of plants can facilitate the development of more intelligent soft robots.

Animals and insects are preferred for biomimetic design because of their mobility; in contrast, plants are regarded as static and passive in nature, as they grow slowly[1]. The tendril of a climbing plant is an example of a curling structure[2–5], and the pinecone enlightens the actuator with an unperceivable motion[6]. There are two strategies for accelerating plant motion: irreversible fracture (*Impatiens glandulifera*) and reversible mechanical instability (*Dionaea muscipula*). The Venus flytrap belongs to a group of carnivorous plants that evolved to catch insects for nutrition. The Venus flytrap is astonishing because of its rapid closure, which distinguishes it from other plants[7].

Due to their rapid closing behavior, motion mechanisms of the Venus flytrap have been explored and applied to design robots[8,9]. Wang et al. proposed a soft microrobot that can curl slowly but with no snapping motion, driven by temperature whose size is $17mm \times 26mm \times 6mm$[10]. Ma et al. presented a thermally response fabricated by liquid metal, whose size is $40mm \times 10mm \times 1.5mm$and response time is 15s[11]. The soft bistable structures[12] designed by Dario et al. respond in 1 s, which is fabricated by hygroscopic electrospun nanofibers and with the size of $17mm \times 11mm \times 0.06mm$. The robot proposed by Zhang et al. could response within 120 s and it is with a size of $16mm \times 2.5mm \times 1.8mm$, which is composed of thermo-responsiveness hydrogels[13]. A light-driven artificial flytrap fabricated by Wani et al. is $5mm \times 1mm \times 0.02mm$big, uses liquid–crystal elastomer and could finish grasping within 2.4s[14]. Schmied et al. presented a Venus flytrap inspired architecture, whose size is $150mm \times 90mm \times 0.25mm$and could bend within 0.2s[15]. Wang et al. presented a bionic Venus flytrap which is powered by pressued gas and with size of $200mm \times 85mm \times 4mm$and whose response time is 2s[16]. As we can see that even though the robots mentioned are all inspired by the Venus flytrap, the closing time and size vary a lot. Some of the robots mimic the morphology of the plant and others are designed for snapping motion. For an artificial Venus flytrap, if there is some rules researchers have to follow and what kind of the geometric size design could help to control the closing time is necessary to discuss. Meanwhile, all these differences are caused by that the Venus flytrap exploits snapping motion to achieve rapid closure, and the underlying mechanism is not fully understood. To instruct the design of the robots, it is essential to uncover how the geometric parameters of the plant would affect the closing time.

Researchers have attempted to explain the mechanism underlying this snapping ability[17–21]. Three groups have published mathematical models since 2005[17]. First, Forterre et al. investigated the snapping motion of the Venus flytrap by marking several fluorescent points on the surface of the plant and recording the closing process using a high-speed camera[17]. After observing the rapid curvature change, they developed a mathematical model that considers the Venus flytrap as a doubly curved leaf, i.e., one that is curved in two orthogonal directions; bending the leaf causes its midplane to be stretched. Even though in their kinetic model, a dimensionless geometric parameter which quantifies the coupling between bending and stretching deformations in terms of the leaf thickness, the leaf length, and the observed curvature of the open leaf might influence the snapping time, a more comprehensive analysis of which parameters are essential for the closing time requires more direct evidence. Second, to explain how this plant achieves snapping, Markin et al. reported that the Venus flytrap has two layers: outer and inner hydraulic layers with different hydrostatic pressures. They mentioned that stimuli open the

Department of Mechanical Engineering, Osaka University, Osaka, Japan. ✉email: morishima@mech.eng.osaka-u.ac.jp

water channel, and water rushes from one layer to another. On the basis of this assumption, they established a mathematical model and calculated the total energy of the process[18,22]. According to their hydroelastic curvature model, the elastic energy stored in the leaf which is related to the curvature would trigger the closing motion and the deformation of the leaf would vary with time. Third, Sachse et al. used a computational model to reproduce the snapping motion[21,23]. They modeled the Venus flytrap as a two-layer (upper epidermis and lower epidermis) or three-layer (upper epidermis, mesophyll, and lower epidermis) structure. However, from biological anatomy, if there are several layers of cells with different morphology is doubtful. Recently, they published another paper in which they used a three-dimensional (3D) digital image correlation imaging system to analyze the strain conditions during the re-opening of the plant and described the Venus flytrap as a single-degree-of-freedom model[20]. Based on the kinetic model they used to explain the snapping, the structure's slenderness which is influenced by the leaf length and thickness should determine the closing motion. All three groups tried to find the connection between the geometric parameters and the closing motion. How should separate parameters such as the leaf thickness, the leaf length, and the curvature or the hybrid parameters such as the dimensionless parameter proposed by Forterre and the slenderness affect the closing time? Then, more samples should be tested for this purpose. Besides, it is worth noting that the Venus flytrap closes quickly (within 0.5 s) but opens slowly (hours without insect hunting and days with hunting). Thus far, for the previous model, only the closing-snapping process could be explained. It has been difficult to interpret both closing and re-opening processes using mathematical models.

The mathematical model could benefit the robot design considering that it would simplify the biological models and explore the key parameters of the model. The fracture of the *Impatiens glanduliferais* irreversible[24], however, the snapping of the Venus flytrap is a buckling phenomenon[21]. Buckling, which involves sudden changes in deformation, is important in structural engineering[25,26]. Although it is sometimes regarded as failure, because large deformations are risky, this principle is applied in structural designs, e.g., for energy harvesters[27–30]. Kurutz presented a detailed equation for the equilibrium paths of buckling[31]. They provided a specific description of the bifurcation equilibrium path and its tangential stiffness under configuration-dependent loading. This asymmetric buckling exhibited the same trend as that of the Venus flytrap.

Previous studies explored the structure of trigger hair by micro-CT[32] and dynamic motion based on high-speed cameras and a 3D digital image correlation imaging system. Micro-CT is feasible to obtain the cellular structure, but the measured area is too small for the whole sample. X-ray CT is an option for the whole plant; however, it is hard to determine cellular composition. Therefore, in this study, the invasive dissection method and the noninvasive laser profiler were combined to understand both cellular and tissular structure. For the dynamic closing and re-opening processes, high-speed cameras require several marking points to track the motion of the leaf which is with lower resolution and efficiency. The 3D digital image correlation imaging system could complete imaging and stress evaluation at the same time, but the time resolution is not enough for the precise closing recording. In the present study, a 3D laser profiler (LJ-X8080, Keyence) was used to examine the 3D static shape of the Venus flytrap in both its open and closed states, as shown in Fig. S1. The 3D laser profiler could measure the 3D information noninvasively, without marks, and with high accuracy. Simultaneously, we recorded the dynamic closing with 500 frames per second and re-opening processes. According to the morphological data, we calculated the mean curvature change and determined the relationship between geometric parameters and dynamic motion variables. The correlation coefficients between the geometric parameters and closing time/closing speed were calculated to determine whether the absolute value of the mean curvature affected the response time. Finally, an asymmetric-bifurcation model was employed to describe the motion of the Venus flytrap, as shown in Fig. 1. The closed and open Venus flytraps had energy differences, and this energy difference controlled the rapid closure and slow re-opening. When the plant was placed at room temperature for dehydration, the energy decreased, and the plant eventually lost its snapping ability.

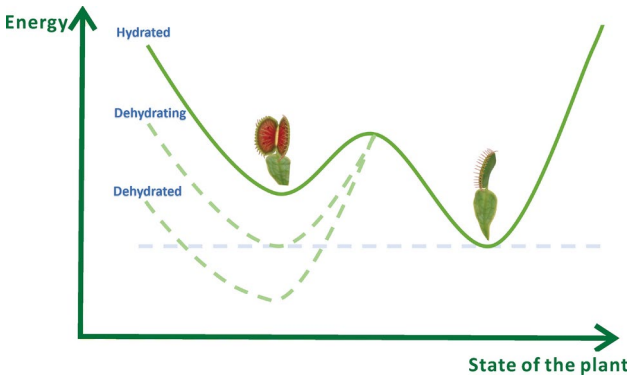

Fig. 1. The energy-changing process of the Venus Flytrap: the open and closed positions had asymmetric energy: there was a difference in elastic potential energy between the opening and closed states. Lower energy benefited rapid closure and higher energy caused the slow re-open process. When the sample was cut from the stem and put at room temperature, the open leaf would dehydrate to decrease energy and could not complete snapping at last.

Results

Morphology of Venus flytrap

The surface shapes of the plants were recorded using a 3D laser profiler. When the leaf was open, the upper epidermis, lower epidermis, and lateral surface were scanned at 500 frames per second (fps) to obtain 3D information. Then, the leaf was fixed at the stem, and the closing process ($N = 67$) was recorded at 500 fps by stimulating the trigger hair twice using forceps. The closing process was continuously recorded, and the scan area was in the middle of the lobe. Using this method, changes in the lateral curve were measured. After closure, the lateral 3D shape was re-scanned. The original data from the Keyence software (LJ-X Observer) are presented in Fig. 2(a). As shown in Fig. 2(b), the data were processed in MATLAB to mesh and contour the images. The curve was plotted for different sections, and the mean curvature was calculated. Contour images can be used to confirm the 3D shape and height information. After closure, the main change occurred in the middle part of the lobes; the lower part near the midrib did not change significantly, similar to a cantilever beam. The x- and y-axis coordinates in Fig. 2(b) are in pixels.

Regarding the data obtained from the 3D laser profiler, the curves parallel and vertical to the midrib were scattered; the curves from these two orthogonal directions are shown in Fig. 3(a). Not like a sphere or a cylinder, the curves in the two orthogonal directions changed continuously from the bottom near the petiole to the tip and from the midrib to the end with teeth. The location and height were applied to fit a surface. And then, the principle curvature, mean curvature, and gauss curvature of the surface were calculated, as shown in Fig. 3(b). In Fig. 3(b), the lateral surface for the opening and closed states was fitted as a smooth surface, whose curvature could be deduced in MATLAB. The fitting error could be found in **Fig.**S2. As shown by the meshing surface of curvatures, the lobes of the plant went through an apparent gauss curvature change. However, in current artificial Venus flytrap[11,33,34], this change was ignored.

To simplify the analysis, the sectional curve vertical to the midrib was examined to check the shape transformation. Two datasets were used to calculate the mean curvature of the lateral surface of the plant. The first was from the recorded dynamic closing process data. The other was the middle curve obtained from the static 3D lateral scanning results. The mean lateral curvatures of the open and closed samples and the curvature change were computed, as shown in Fig. 4(a). The absolute value of the open state was smaller than that of the closed state for both the dynamic closing data and static lateral data.

Meanwhile, from the open samples' upper epidermis and lower epidermis (Fig. S3 shows all the upper and lower curves), the height and width of the intact leaves were calculated, and from the upper curve, the height and width distributions were obtained as shown in Fig. 4(b). According to the model proposed by Forterre et al., the closing time is dominated by the thickness of the lobe. However, it is impossible to determine the thickness directly using a 3D laser profiler. Therefore, some of the samples were dissected using a vibratome, and the basic geometric parameters were acquired from optical images, as shown in Fig. S4. Fig. 5 presents the distributions of the leaf height (L), width (W), and thickness (T) obtained from the section samples. Fig. S5 shows the correlation heatmap of these three parameters; the thickness was strongly correlated with the width, as shown in Fig. 5(b). The thickness had a positive linear relationship with the width. Additionally, the ratio of the total length of the lobe ($L_T = \sqrt{L^2 + W^2}$) to the thickness was calculated as 12.1 ± 1.36 for closed samples and 12.1 ± 1.22 for open samples. This ratio affects the snapping motion in the model proposed by Poppinga et al. This ratio revealed the slenderness of the sample, and the higher the value is, the easier the sample snaps. The samples used by Poppinga et al. had median slenderness values of 38.67 and 44.74 for N (normal size) and L (large size) morphotypes respectively, but their slenderness values have a high variation. For our samples, this ratio is smaller than theirs, although the calculation method is a little bit different.

Dynamic motion of Venus flytrap

Closing process

The lateral curves with respect to time during closing are plotted in Fig. 6(a). Supplementary video 1 shows the dynamic motion, in which the change of the lateral curve and the route tracking by TrackMate in ImageJ could be inspected. The closing curve changed rapidly, indicating that snapping occurred. The mean curvature of each frame was calculated. As shown in Fig. 6(b), the mean curvature maintained in the first stage decreased suddenly and finally stabilized. To test the closing time quantitatively, the Gompertz model was applied to fit the scatterers.

$$f(t) = d + (a - d)e^{-e^{-b(t-c)}}$$

In this equation, $\lim_{t \to -\infty} f(t) = a$, $\lim_{t \to +\infty} f(t) = d$, and the amplitude $A = a - d$. The middle 80% of the area is used to define the closing time.

$$\Delta t = t_{|f(t)=d+0.1A} - t_{|f(t)=a-0.1A}$$

The red pentagons indicate the closing period. For all the samples, $N = 67$ dynamic closing processes were recorded. The relationship between the amplitude of the curvature and closing time is shown in Fig. 6(c). The closing time did not decrease with an increase in the mean curvature amplitude. Comparing the outlier and normal samples revealed that the outliers closed smoothly, as shown in Fig. 6(d). For the snapping motion, the closing angle changed quicker and quicker; however, for the smooth motion, the angle changed with the same speed. As indicated by **Fig.** S6, the absolute value of the mean curvature of the open state was smaller than that of the closed state, which is consistent with the asymmetric closing and re-opening behavior.

To avoid the influence of fitting, the correlations between the mean curvature (curvature of the upper, lower, and lateral curves for open and closed samples), leaf size (length, height and width acquired from the upper

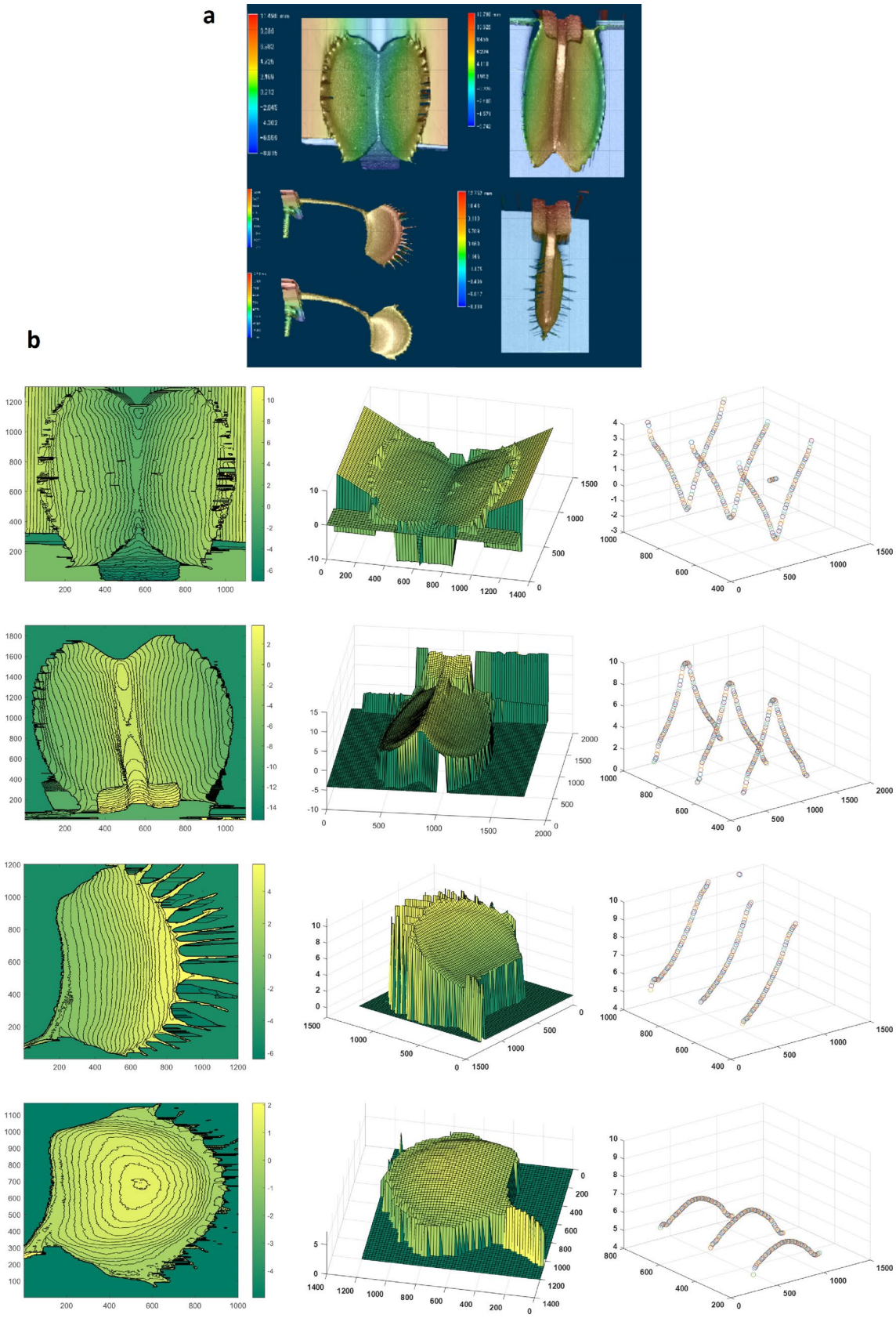

Fig. 2. 3D morphology of the plant obtained from laser profiler and processed by Matlab: (**a**) The original data was obtained from the 3D laser profiler. (**b**) The contour and meshing images of the Venus Flytrap: the upper epidermis, the lower epidermis, and the lateral surface for open and closed states. The section curves could be used for the mean curvature calculation. The units of the x and y axis were pixel and the z axis was mm based on the laser profiler.

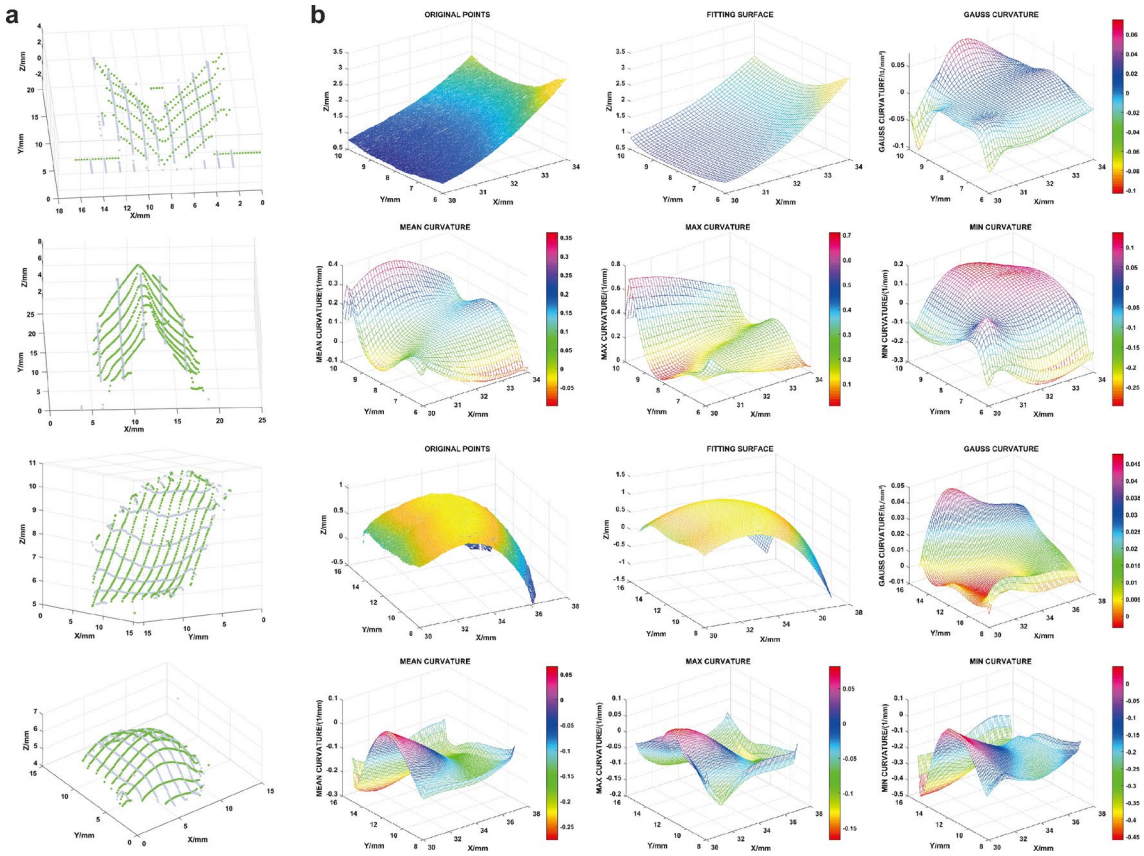

Fig. 3. The 3D surfaces fitted in the MATLAB and curvature calculation of the lateral surface: (**a**) The first column: The figures from top to bottom are the upper epidermis, the lower epidermis, the opening lateral surface, and the closed lateral surface respectively. The surfaces are presented by curves in vertical and parallel directions to the midrib. The curves in both directions show the shape and curvature change. (**b**) The second, third and fourth columns. The Gauss curvature ($k_1 \cdot k_2$), mean curvature ($(k_1 + k_2)/2$), and principal curvature (maximum curvature k_1 and minimum curvature k_2) of fitted surfaces. The first two rows display the opening lateral surface information: the original data was used for the fitting surface, and then the curvature of the fitting surface was calculated. Instead of the mean curvature or Gauss curvature of the whole curve, the curvature of every point could be computed for detailed analysis. The last two rows display the closed lateral surface information: compared with the opening surface results, it could be found that the mean curvature and Gauss curvature changed a lot.

curve), and closing time were analyzed. The correction coefficients are shown in Fig. 7, from which it can be concluded that the closing time is not strongly related to any of the known parameters.

In the modelling results of Forterre et al.[17], the closing time was related to the thickness of the plant. The thickness could not be easily determined without damaging the plant, which is why section samples were used to assess the relationship between the thickness and easily obtained parameters, such as the length and width of the plant. As shown in Fig. 5(b), the thickness increased with the width. Meanwhile, Forterre et al. also mentioned a mixed parameter $\alpha = \frac{L^4 k^2}{h^2}$, in which $L = \frac{lenght+height}{4}$, k means the mean curvature of the opening leaf, and h is the thickness of the leaf. Even though the thickness of the leaf can not be measured directly by our method, the linear relationship between the width and the thickness could be utilized for calculation. Then the revised $\alpha = \frac{(length+heigh)^4 k^2}{w^2}$, in which w is the width of the leaf. As shown in Fig.S7, it could be found that the closing time would not be influenced by the revised α. Nevertheless, the width and leaf size L have a linear relationship, which meets the conclusion obtained by Forterre et al. that the ratio between leaf size and thickness was constant.

In our samples, the closing time did not change with respect to these geometric parameters. This may be due to the resolution of the measurement and the definition of the closing time. According to our results, similar to the all-or-none reaction of the action potential, the snapping behavior exhibited an all-or-none phenomenon. Once the plant was standing by (finish energy storage in the process of reopening) and the stimuli were sufficient to trigger the motion, it would snap (only 2 of 67 plants closed smoothly). Furthermore, it could not stop in the intermediate state from open to closed, and a sudden jump occurred. In the snaping, the geometric parameters may influence the energy we have to overcome to trigger the motion, but they have no impact on the closing time.

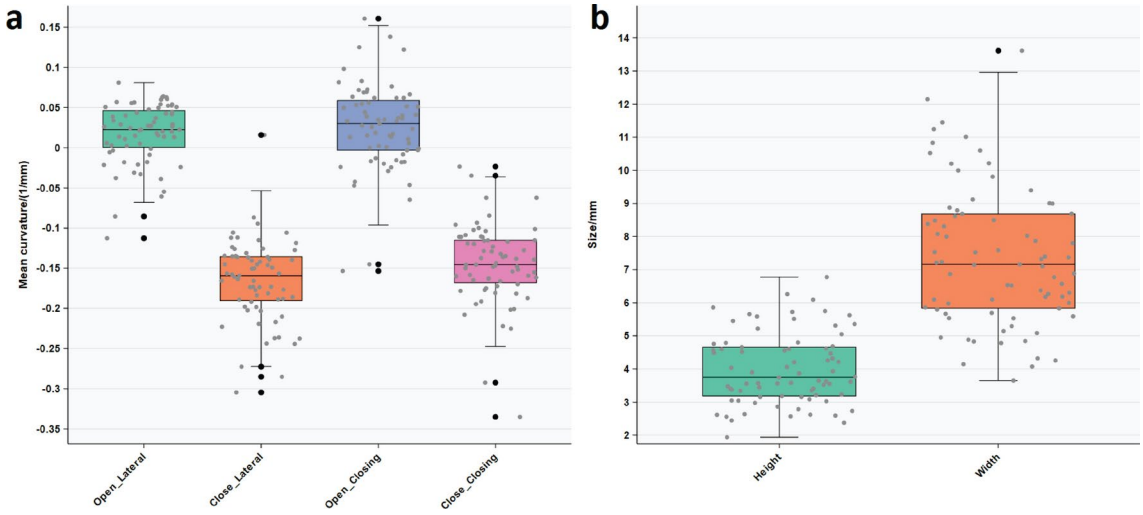

Fig. 4. The mean curvature and the size of samples: (**a**) The mean curvature distribution: as shown in the third and fourth rows of Fig. 2 (b), 3D static information of the surface was scanned and the Open-Lateral and Close-Lateral meant the mean curvature calculated from the lateral curve (the curve like the third column, and the curve in the central part was utilized for calculation) for open and closed samples. Meanwhile, during the dynamic closing process recording, the lateral curve in the central part was also measured and Open-Closing and Close-Closing meant the mean curvature calculated from the closing process when the sample is open or closed. The absolute value of the mean curvature of the open samples was bigger than the closed ones. (**b**) The height and width information was obtained by the upper curve.

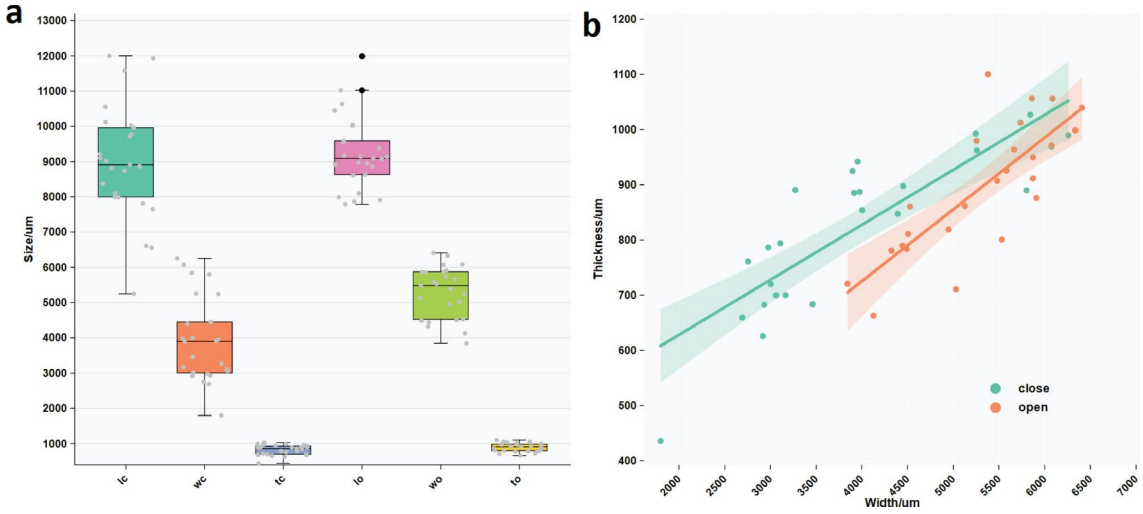

Fig. 5. The size of the plant and the relationship between leaf width and thickness: (**a**) Leaf size distribution: lc-length of the closed samples, wc-width of the closed samples, tc-thickness of the closed samples, lo-length of the open samples, wo-width of the open samples, to-thickness of the open samples. (**b**) The relationship between the width and thickness of the leaves: the thickness would increase by the width.

The speed of the plant was defined as half the width divided by the closing time, and the corresponding correlation coefficient is shown in Fig. S8. Because time was not related to other parameters, the speed increased with the width of the lobes. The increased speed might be caused by the bigger turgor pressure, which would be influenced by the cell volume, cell number, cell wall stiffness, and chemical concentrations. The possible factors would be measured and discussed in future work. In the model from Sachse et al.[21], they mentioned hydraulic pressure differences would cause prestress of the leaf. The speed calculated here was the mean speed during the closing, the acceleration of the leaf must be deduced if we want to test the prestress of the plant from data in this study.

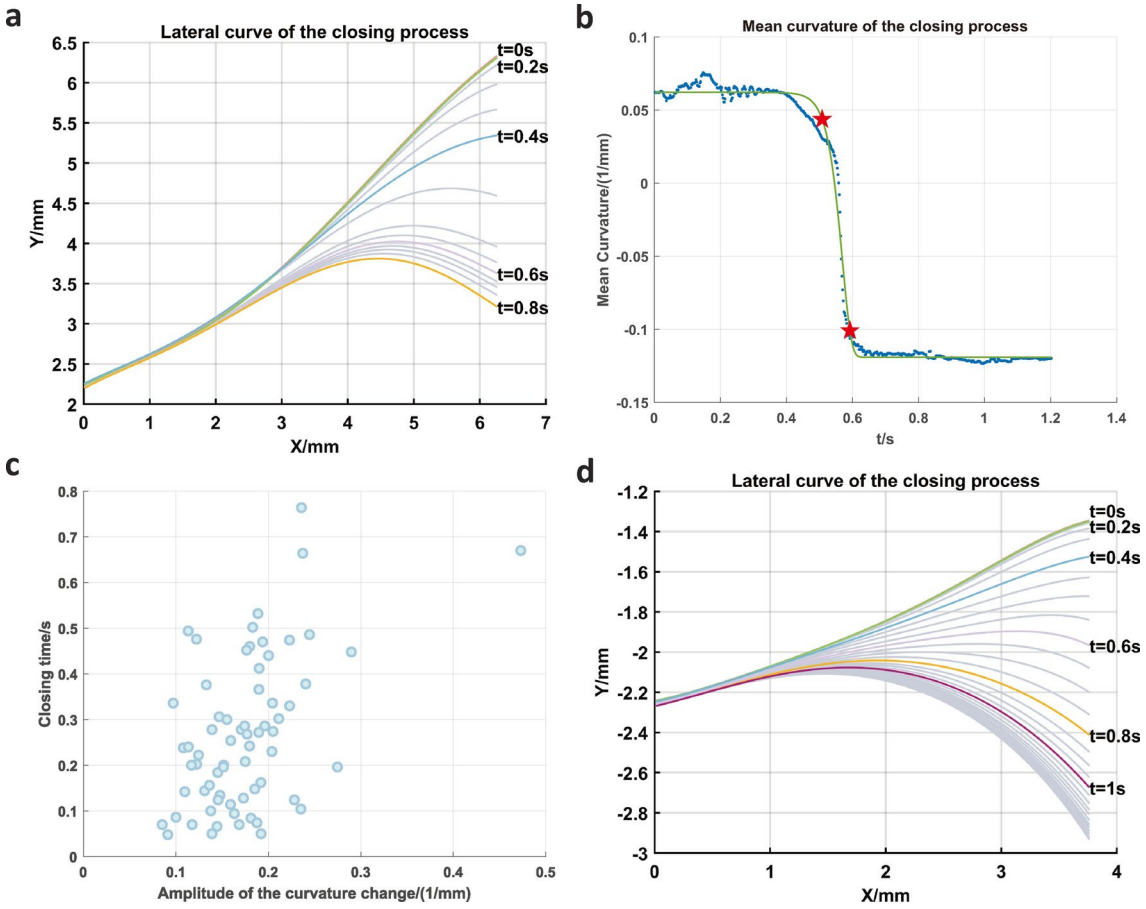

Fig. 6. The closing process and closing time definition: (**a**) The lateral curves changed over time for the sample with snapping motion: the curve would change quickly in a period. The closing happened from t = 0.2 s to t = 0.6 s quickly. (**b**) The mean curvature changing during the closure: the red pentagon represented the upper 10% and lower 10%. (**c**) The scattering for the amplitude of the curvature change and closing time. (**d**) The lateral curves for the sample without snapping: the lobe closed smoothly. The distance from t = 0.4 s to t = 0.6 s was similar to the distance from t = 0.6 s to t = 0.8 s.

Re-opening process

As reported by Poppinga et al., the re-opening process had to be sufficiently slow to store energy and digest insects[20,35]. The re-opening motion of the Venus flytrap was recorded by the 3D laser profiler ($N = 6$). After the closing motion was triggered, the lateral surface was scanned every hour for 48 h, as shown in Supplementary video 2. As shown in Fig. 8(a), the lateral surface was contoured, and the shape remained almost constant, after which the lobe started to open. Similar to the closing process, motion occurred mostly in the middle and top areas. Subsequently, the lateral and mean curvatures were calculated. In Fig. 8(b), the colored bar represents the curvature. Fig 9 shows the mean curvature change. The mean curvature is almost maintained at the same negative value, indicating that the plant remained in a closed state. Approximately 15 h later, the plants began to open, and the mean curvature increased until 30 h after closure, when it returned to a positive value. There were individual differences among the samples, but the re-opening process exhibited the same trend as the closing process, except for the timescale. Similarly, the absolute value of the mean curvature after opening was smaller than that after opening.

Asymmetric-bifurcation model of Venus flytrap

Spring-actuated jumping systems are always adopted to explain the process that insects first latch their legs in place and then slowly contract muscles that store muscle work in elastic cuticular structures[36,37]. The elastic energy could be released to actuate leg extension. Similar to this kind of energy system, plants could store energy by their turgor pressure or cell wall stiffness[38,39]. In both the closing and re-opening process, the curvature of the closed state had a larger absolute value than that of the opening state, which indicated the asymmetries. Therefore, a mathematical model that exhibits these characteristics is crucial. Asymmetric bifurcation of the buckling model is used to explain the Venus flytrap model. As shown in Fig. 10, instead of the symmetric model used by Durak et al.[20], the lobe was connected to an inclined spring, which caused asymmetric equilibrium paths in our model.

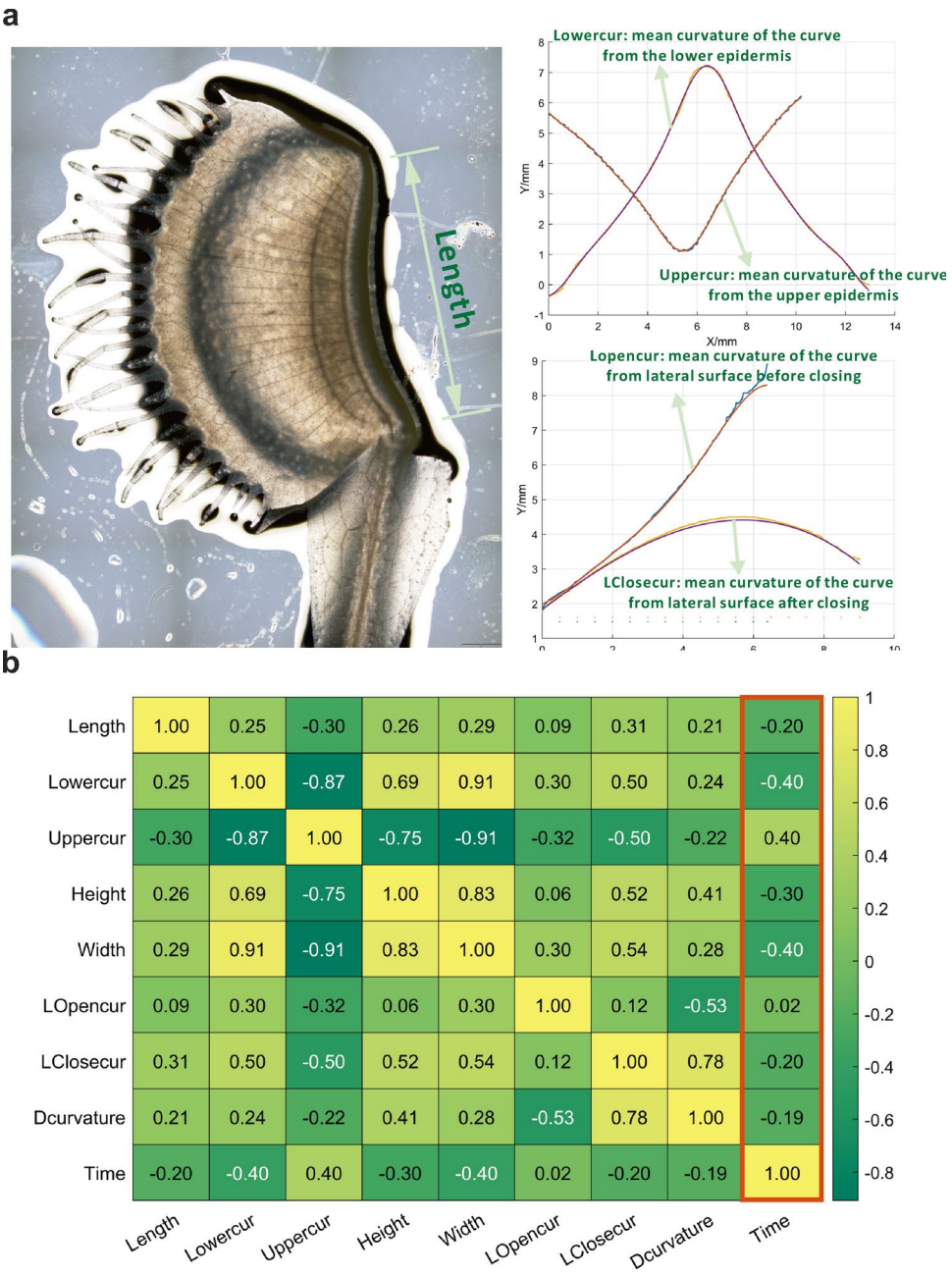

Fig. 7. The correlation coefficient between geometric parameters and the closing time: (**a**) The length of the Venus flytrap. (**b**) The meaning of all parameters. Lowercur-mean curvature calculated from the lower curve, Uppercur-mean curvature calculated from the upper curve, Height and width were acquired from the upper curve, LOpencur-mean curvature from the lateral curve when the sample was open, LClosecur-mean curvature from the lateral curve when the sample was closed, Dcurvature-the difference of the mean curvature between open and closed curve, and Time-closing time defined by Gompertz model. c. The correlation heat map for the closing time and geometry parameters.

In Fig. 10, the model is modified to a cantilever ( ) that is skewly supported by a spring, whose length is $L = \alpha l$. For the spring, $B = c\omega$, where B represents the force of the spring, c is the spring constant, and $\omega = l(\sqrt{1+\alpha^2+2\alpha sinq} - \sqrt{1+\alpha^2})$ represents the elongation of the spring, with $q$being the rotation angle of the cantilever[31]. The external force $F = \lambda F_0 + fu$ changed with the vertical deformation u. The values of F_0 and f were defined in each case.

In the case of a dead load, the load is not related to the deformation of the cantilever and the fundamental equilibrium path is given by the classical expression

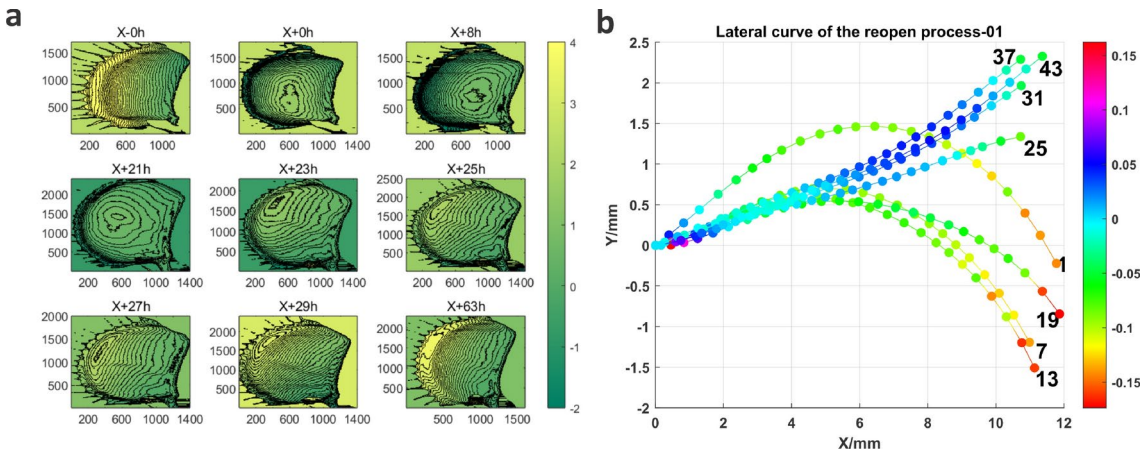

Fig. 8. The reopening process of the Venus flytrap: (**a**) The contour images during re-open process: X-0 h was the open state, x + 0 h was the sample triggered to close, and then the sample would be scanned every hour for 48 h. After 48 h, the sample would be scanned again at 63 h. (**b**) The lateral curves during the re-open process: the color bar indicated the curvature, and the number showed how many hours after the closing. The main moving parts were the middle and upper parts.

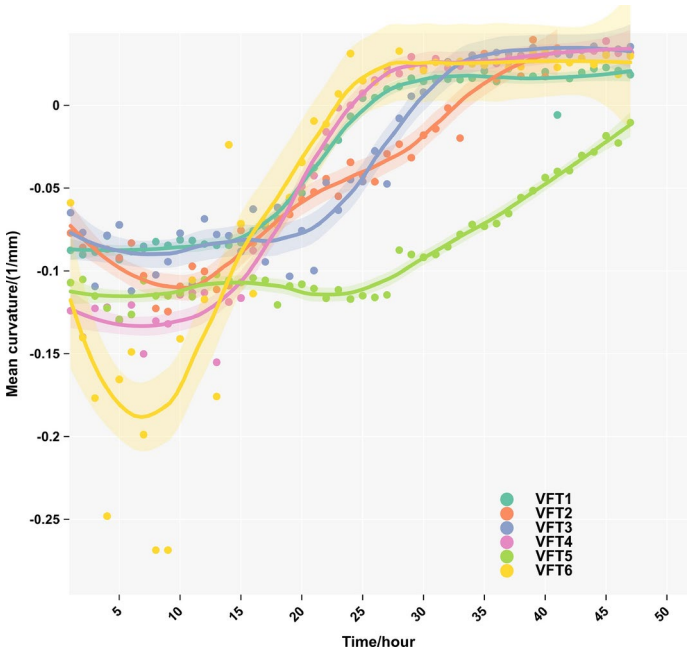

Fig. 9. The mean curvature changes of the re-open process for all six samples: The curvature kept for approximately 15 h, and then the sample began to open. The re-open process shared a similar trend with the closing process, but the time scale was bigger.

$$\lambda(q) = \frac{cl}{F}\frac{\alpha}{tanq}\left(1 - \sqrt{\frac{1+\alpha^2}{1+\alpha^2+2\alpha sinq}}\right) \quad \lambda_{cr} = \pm\frac{cl}{F_0}\frac{\alpha^2}{1+\alpha^2} \quad , \tag{1}$$

where λ_{cr} represents the asymmetric-bifurcation point at $q = 0$ and $q = \pm\pi$.

For the dead load ($f = 0$), the associated classical function $K(q)$ of the tangent stiffness was as follows when we selected $c = 1, l = 1, F_0 = 1$, and $\alpha = 2$:

$$K(q) = cl^2\left[\alpha^2 cos^2 q\sqrt{\frac{1+\alpha^2}{(1+\alpha^2+2\alpha sinq)^3}} - \frac{\alpha}{sinq}\left(1 - \sqrt{\frac{1+\alpha^2}{1+\alpha^2+2\alpha sinq}}\right)\right]. \tag{2}$$

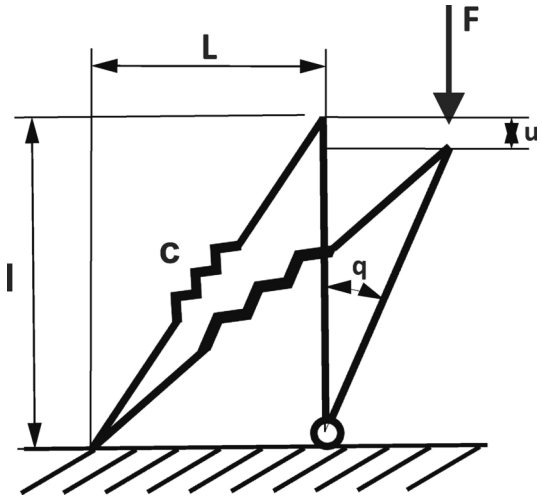

Fig. 10. The asymmetric bifurcation model that a cantilever connected with an inclined spring. The Venus flytrap has three positions- position one was the open state, position two was the position where the spring was unstretched, and the position three was the closed state.

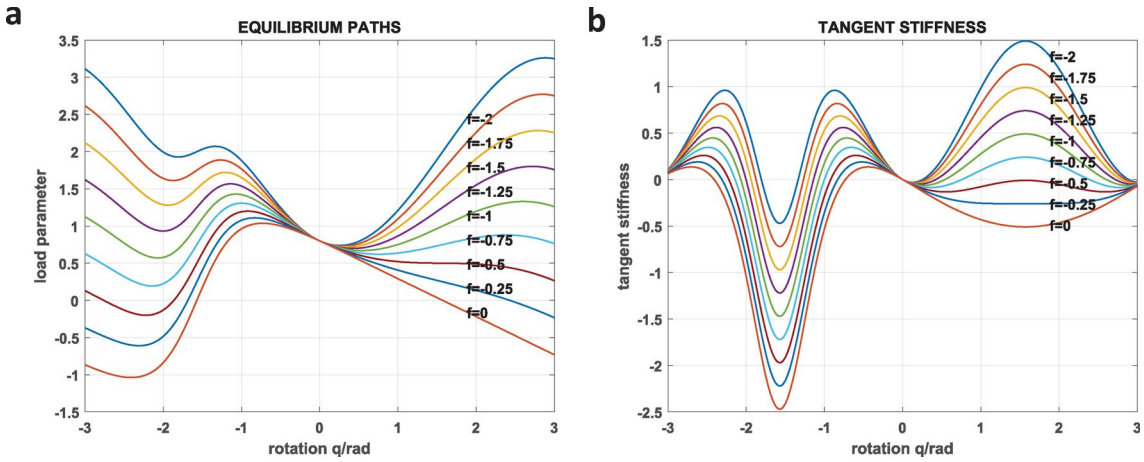

Fig. 11. (**a**) The equilibrium paths of the asymmetric bifurcation model for different f values. The x-axis was the rotation angle of the cantilever and the y-axis was the equilibrium path. (**b**) The tangent stiffness of the model.

For a linear variable load, the post-bifurcation equilibrium paths are expressed as follows:

$$\lambda(q) = \frac{l}{F_0}\left[\frac{c\alpha}{tanq}\left(1 - \sqrt{\frac{1+\alpha^2}{1+\alpha^2+2\alpha sinq}}\right) - f(1 - cosq)\right] \tag{3}$$

$$\lambda_{cr} = \frac{cl}{F_0}\frac{\alpha^2}{1+\alpha^2} \quad \lambda_{cr} = \frac{l}{F_0}\left(c\frac{\alpha^2}{1+\alpha^2} - 2f\right) \tag{4}$$

with the same asymmetric-bifurcation point at the critical point at $q = 0$ and different asymmetric-bifurcation points at $q = \pm\pi$. The associated tangent stiffness function is expressed as follows:

$$K(q) = cl^2\left[\alpha^2 cos^2 q\sqrt{\frac{1+\alpha^2}{(1+\alpha^2+2\alpha sinq)^3}} - \frac{\alpha}{sinq}\left(1 - \sqrt{\frac{1+\alpha^2}{1+\alpha^2+2\alpha sinq}}\right)\right] - fl^2 sin^2 q. \tag{5}$$

To identify the influence of the external load and simplify the calculation, in the model, the parameters were set as $c = 1, l = 1, F_0 = 1$, and $\alpha = 2$. The relationship between the rotation angle and equilibrium path is shown in Fig. 11. The exact value of this parameter will be determined in a future study.

For the Venus flytrap, the original vertical position of the mathematical model with an unstretched spring was an intermediate state. The closed state was the equilibrium position near the original position, and the open state was a position farther from it. The energy of the system E can be increased by the work done by an external

force $W = Fu$; thus, larger vertical deformation of the equilibrium path corresponds to a larger amount of energy stored in the system. Owing to the asymmetric positions of the two states, their energies differed. The slow re-opening was caused by higher energy in the open state. When the samples were dehydrated, the energy decreased until it was lower than that of the closed sample, as shown in Fig. 1. During the reopening process, the system requires more energy storage (from the hydraulic pressure or stress in the cell wall) and the closing process would utilize the stored energy for quick snapping.

Conclusion

Using a 3D laser profiler, static 3D information of a Venus flytrap in the open and closed states was acquired, and the dynamic closing and re-opening processes were recorded. According to the shape data, a contour map was employed to describe the 3D information of the plant, and the mean curvature during closure and re-opening was calculated. The correlation coefficients between the closing time and leaf geometric parameters were analyzed. Finally, a mathematical bifurcation model was used to explain the asymmetric motion of the plant.

The open and closed states exhibited similar curvature change trends over time. However, they had different mean curvatures and timescales, indicating energy differences. During closure, snapping and smooth motion were observed. Moreover, the closing time was not strongly correlated to any other geometric parameter, and the plant snapped from the open position to the closed position once the stimuli were sufficiently strong to trigger motion. It could not stop at the intermediate position, and the closure was all-or-none, similar to the action potential. A mathematical buckling model with asymmetric equilibrium paths explained the rapid closure and slow re-opening motion of the Venus flytrap. The conclusion that the closing time is not related to the geometric parameters can inspire a minimized soft robot and the linear relationships between some parameters could instruct the design of the artificial Venus flytrap. Despite the current conclusion being limited to robot design because it is still uncertain why the closing time is not related to the geometric parameters; this phenomenon should be considered when the artificial Venus flytrap is proposed.

Data availability

The datasets generated and/or analyzed during the current study are available in the figshare repository at https://figshare.com/articles/dataset/keyence_shape_sensor_data/25678779

Received: 11 April 2024; Accepted: 3 December 2024
Published online: 08 February 2025

References

1. Speck, T. et al. Plants as inspiration for material-based sensing and actuation in soft robots and machines. *MRS Bull.* **48**, 730–745 (2023).
2. Meder, F., Murali Babu, S. P. & Mazzolai, B. A plant tendril-like soft robot that grasps and anchors by exploiting its material arrangement. *IEEE Robot. Autom. Lett.* **7**, 5191–5197 (2022).
3. Cheng, Y. et al. A biomimetic conductive tendril for ultrastretchable and integratable electronics, muscles, and sensors. *ACS Nano*. **12**, 3898–3907 (2018).
4. Wu, H., Zheng, Y. & Zeng, Y. Fabrication of helical nanofibers via co-electrospinning. *Ind. Eng. Chem. Res.* **54**, 987–993 (2015).
5. Guo, X. et al. Encoded sewing soft textile robots. *Sci. Adv.* **10**, eadk3855 (2024).
6. Zhang, F. et al. Unperceivable motion mimicking hygroscopic geometric reshaping of pine cones. *Nat. Mater.* **21**, 1357–1365 (2022).
7. Hodick, D. & Sievers, A. On the mechanism of trap closure of Venus flytrap (Dionaea muscipula Ellis). *Planta*. **179**, 32–42 (1989).
8. La Porta, C. A. M. et al. Metamaterial architecture from a self-shaping carnivorous plant. *Proc. Natl. Acad. Sci.* **116**, 18777–18782 (2019).
9. Westermeier, A. S. et al. How the carnivorous waterwheel plant (Aldrovanda vesiculosa) snaps. *Proc. R. Soc. B Biol. Sci.* **285**, 20180012 (2018).
10. Wang, X., Gao, Y., Ma, X., Li, W. & Yang, W. A bionic venus flytrap soft microrobot driven by multiphysics for intelligent transportation. *Biomimetics*. **8**, 429 (2023).
11. Ma, B., Xu, C., Cui, L., Zhao, C. & Liu, H. Magnetic printing of liquid metal for perceptive soft actuators with embodied intelligence. *ACS Appl. Mater. Interfaces*. **13**, 5574–5582 (2021).
12. Lunni, D., Cianchetti, M., Filippeschi, C., Sinibaldi, E. & Mazzolai, B. Plant-inspired soft bistable structures based on hygroscopic electrospun nanofibers. *Adv. Mater. Interfaces*. https://doi.org/10.1002/admi.201901310 (2020).
13. Zhang, Z. et al. Bioinspired bilayer structural color hydrogel actuator with multienvironment responsiveness and survivability. *Small Methods*. https://doi.org/10.1002/smtd.201900519 (2019).
14. Wani, O. M., Zeng, H. & Priimagi, A. A light-driven artificial flytrap. *Nat. Commun.* https://doi.org/10.1038/ncomms15546 (2017).
15. Schmied, J. U., Le Ferrand, H., Ermanni, P., Studart, A. R. & Arrieta, A. F. Programmable snapping composites with bio-inspired architecture. *Bioinspir. Biomim.* https://doi.org/10.1088/1748-3190/aa5efd (2017).
16. Wang, Y., Yan, J., Li, J., Huang, M. & Luan, Z. The fabrication of gas-driven bionic soft flytrap blade and related feasibility tests. *J. Bionic Eng.* **20**, 628–644 (2023).
17. Forterre, Y., Skotheim, J. M., Dumais, J. & Mahadevan, L. How the Venus flytrap snaps. *Nature*. **433**, 421–425 (2005).
18. Markin, V. S., Volkov, A. G. & Jovanov, E. Active movements in plants. *Plant Signal. Behav.* **3**, 778–783 (2008).
19. Volkov, A. G., Forde-Tuckett, V., Volkova, M. I. & Markin, V. S. Morphing structures of the Dionaea muscipula ellis during the trap opening and closing. *Plant Signal. Behav.* **9**, e27793 (2014).
20. Durak, G. M. et al. Smooth or with a Snap! Biomechanics of trap reopening in the venus flytrap (Dionaea muscipula). *Adv. Sci.* **9**, 2201362 (2022).
21. Sachse, R. et al. Snapping mechanics of the Venus flytrap (Dionaea muscipula). *Proc. Natl. Acad. Sci.* **117**, 16035–16042 (2020).
22. Volkov, A. G., Murphy, V. A., Clemmons, J. I., Curley, M. J. & Markin, V. S. Energetics and forces of the Dionaea muscipula trap closing. *J. Plant Physiol.* **169**, 55–64 (2012).
23. Poppinga, S. & Joyeux, M. Different mechanics of snap-trapping in the two closely related carnivorous plants *Dionaea muscipula* and *Aldrovanda vesiculosa*. *Phys. Rev. E*. **84**, 041928 (2011).
24. Deegan, R. D. Finessing the fracture energy barrier in ballistic seed dispersal. *Proc. Natl. Acad. Sci.* **109**, 5166–5169 (2012).
25. Hutchinson, J. W. Plastic Buckling. In *Advances in Applied Mechanics* (ed. Yih, C.-S.) vol. 14 67–144 (Elsevier, 1974).

26. Supple, W. J. A general theory of elastic stability. *Aeronaut. J.* **79**, 274–274 (1975).
27. Zhou, H. et al. Stretchable piezoelectric energy harvesters and self-powered sensors for wearable and implantable devices. *Biosens. Bioelectron.* **168**, 112569 (2020).
28. Liu, Q., Qin, W., Yang, Y. & Zhou, Z. Harvesting weak vibration energy by amplified inertial force and multi-stable buckling piezoelectric structure. *Mech. Syst. Signal Process.* **189**, 110125 (2023).
29. Bi, H., Wang, B., Huang, Y., Zhou, J. & Deng, Z. Nonlinear dynamic performance of buckled piezoelectric ribbon-substrate energy harvester. *Compos. Struct.* **261**, 113570 (2021).
30. Liu, Q. & Qiao, P. Buckling analysis of bilayer beam-columns with an asymmetric delamination. *Compos. Struct.* **188**, 363–373 (2018).
31. Kurutz, M. Modification of the structural tangent stiffness due to nonlinear configuration-dependent conservative loading. *Comput. Assist. Mech. Eng. Sci.* **3**, 367–388 (1996).
32. Wang, K. et al. Biomechanics on ultra-sensitivity of Venus Flytrap's micronewton trigger hairs. *Adv. Sci.* **11**, 2405544 (2024).
33. Wang, Y. Z., Gupta, U., Parulekar, N. & Zhu, J. A soft gripper of fast speed and low energy consumption. *Sci. China Technol. Sci.* **62**, 31–38 (2019).
34. Temirel, M. et al. Three-dimensional-printed carnivorous plant with snap trap. *3D Print. Addit. Manuf.* **3**, 245–251 (2016).
35. Poppinga, S., Kampowski, T., Metzger, A., Speck, O. & Speck, T. Comparative kinematical analyses of Venus flytrap (Dionaea muscipula) snap traps. *Beilstein J. Nanotechnol.* **7**, 664–674 (2016).
36. Patek, S. N., Dudek, D. M. & Rosario, M. V. From bouncy legs to poisoned arrows: elastic movements in invertebrates. *J. Exp. Biol.* **214**, 1973–1980 (2011).
37. Sutton, G. P. et al. Why do large animals never actuate their jumps with latch-mediated springs? Because they can jump higher without them. *Integr. Comp. Biol.* **59**, 1609 (2019).
38. Kroeger, J. H., Zerzour, R. & Geitmann, A. Regulator or driving force? The role of turgor pressure in oscillatory plant cell growth. *PLoS ONE*. **6**, e18549 (2011).
39. Chaplain, M. A. J. The strain energy function of an ideal plant cell wall. *J. Theor. Biol.* **163**, 77–97 (1993).

Acknowledgements

This study was supported by the JST SPRING (Grant Numbers J219713005), KAKENHI (Grant Numbers 21K18700 and 22H04951), Tomoaki Mizuno (for Leica VT1000 S), Yuri Terao (for FV3000, Olympus), and the Center for Medical Research and Education, Graduate School of Medicine, Osaka University.

Author contributions

X.Z. conceived ideas and was responsible for all experiments. Y.W. gave experimental instructions. K.M. supervised all experiments and data analysis.

Funding

JST SPRING,J219713005,KAKENHI,21K18700,22H04951

Declaration

Competing interests

The authors declare no competing interests.

Plant guideline

The plants were purchased from Isehana Iris Garden Co., Ltd. http://isehana.com and Maeda Shojiro was responsible for identifying the plant. The voucher specimen was stored at the Medicinal Plant Garden, Graduate School of Pharmaceutical Sciences, Osaka University http://www0.phs.osaka-u.ac.jp/syokubutuen/. If there are any sample requirements, please email the corresponding author. This study complies with the IUCN Policy Statement on Research Involving Species at Risk of Extinction and the Convention on the Trade in Endangered Species of Wild Fauna and Flora.

Additional information

Supplementary Information The online version contains supplementary material available at https://doi.org/10.1038/s41598-024-82156-6.

Correspondence and requests for materials should be addressed to K.M.

Reprints and permissions information is available at www.nature.com/reprints.

Publisher's note Springer Nature remains neutral with regard to jurisdictional claims in published maps and institutional affiliations.